RSC Advances

RSC Publishing

PAPER

View Article Online
View Journal | View Issue

Self-assembly in surfactant-based mixtures driven by acid–base reactions: bis(2-ethylhexyl) phosphoric acid–*n*-octylamine systems

Cite this: *RSC Advances*, 2013, **3**, 5148

Pietro Calandra,*[a] Andrea Mandanici[b] and Vincenzo Turco Liveri[c]

Structural and dynamic features of bis(2-ethylhexyl) phosphoric acid (HDEHP)–*n*-octylamine (NOA) mixtures as a function of the NOA mole fraction (X_{NOA}) have been investigated by SAXS, WAXS, IR, dielectric spectroscopy and polarized optical microscopy. In the $0 \leqslant X_{NOA} < 0.5$ range, mixtures are transparent liquids, while the abrupt formation of a waxy solid characterized by an hexagonal bidimensional structure occurs at $X_{NOA} = 0.5$. Such a composition-induced phase transition results from the synergetic effect of the progressive increase in number density of ordered HDEHP–NOA nanodomains with X_{NOA}. Mainly driven by an HDEHP to NOA proton transfer, the increase of structural order with X_{NOA} arises from the progressive substitution of loosely hydrogen bonded HDEHP–HDEHP aggregates with strongly bonded NOA–HDEHP ones. Analysis of SAXS patterns at temperatures in the 10–70 °C range emphasized that these local structures are scarcely impacted by an increase of thermal fluctuations. Effects due to the steric compatibility between HDEHP and NOA apolar moieties have been highlighted. Overall, the results allow us to emphasize the role of specific polar and apolar interactions joined to steric effects in regulating the molecular organization in surfactant mixtures and can be used to design novel materials with planned physico-chemical properties.

Received 12th December 2012,
Accepted 24th January 2013

DOI: 10.1039/c3ra23295f

www.rsc.org/advances

Introduction

Pure liquid surfactants are characterized by locally ordered structures that exist for a system-dependent time scale together with a molecular diffusion taking place on a longer time scale. Such a peculiarity arises from the typical structure of surfactant molecules which possesses a small polar or ionic group and an elongated apolar (usually alkyl chain) part. In competition with the thermal effect tending to randomize molecular orientation and/or position, the different strengths of the polar–polar, apolar–apolar and polar–apolar interactions drive molecular assembly and lead to a variety of local structures which can be characterized by their mean size, number density and lifetime. These features control the macroscopic physico-chemical properties and are at the basis of specialized biological and technological applications.[1,2]

The variety of materials which can be realized by changing the nature of the hydrophilic group or the length of the alkyl chain can be widely amplified by adopting a bio-inspired strategy based on the mixing of already-known surfactants.

In fact, living systems are characterized by a melange of substances able to form dynamic structures at hierarchical levels of complexity, all contributing to their fascinating functionalities.

Driven by these considerations, we have previously investigated the basic principles of molecular self-assembly reporting the peculiar physico-chemical properties of binary mixtures formed by bis(2-ethylhexyl)phosphoric acid and bis(2-ethylhexyl)amine,[3] and by octanoic acid and bis(2-ethylhexyl)amine.[4,5] These studies allowed us to highlight the role of the acid/basic character of surfactant polar groups to drive proton transfer involving a significant strengthening of the local structures. Interestingly, the emergence of novel structural and dynamic features has been highlighted. Moreover, some hints on the role of the surfactant apolar parts in determining the degree of order of the specific surfactant mixture have been suggested.

In order to extend our knowledge on the effect of the apolar parts of the two surfactants we have decided to investigate some of the physico-chemical properties of bis(2-ethylhexyl) phosphoric acid (HDEHP)–*n*-octylamine (NOA) binary mixtures in all the monophasic composition ranges. The molecular structures of these substances are schematically represented in Fig. 1. It is worth noting that the nature of the

[a]*CNR-IPCF, Consiglio Nazionale delle Ricerche-Sede di Messina, Via Ferdinando Stagno d'Alcontres, 37-98158 Messina, Italy. E-mail: calandra@me.cnr.it; Fax: +39 090 3974130; Tel: +39 090 39762 223*
[b]*Dipartimento di Fisica-Università di Messina, Viale Ferdinando Stagno d'Alcontres, 31-98166 Messina, Italy. Tel: +39 090 6765011*
[c]*Dipartimento di Chimica "Stanislao Cannizzaro", Università degli Studi di Palermo, Viale delle Scienze I-90128, Palermo, Italy. Tel: +39 091 6459844*

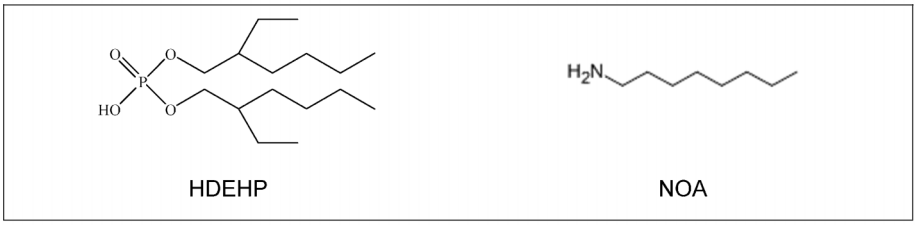

Fig. 1 Schematic representation of HDEHP (left) and NOA (right) molecular structures.

polar groups of bis(2-ethylhexyl) phosphoric acid and *n*-octylamine is well-suited to allow proton transfer involving head-to-head associations, whereas the single alkyl chain of the amine molecule should involve enhanced adaptability within the HDEHP local structure.

Experimental part

n-Octylamine (NOA, Aldrich >99.5%) and bis(2-ethylhexyl)phosphoric acid (HDEHP, Aldrich 97%) were used as received. NOA–HEDHP mixtures were prepared by weight and stored in sealed vials. Their composition hereafter is expressed as the NOA molar fraction (X_{NOA}).

Preliminary experiments showed that the progressive addition of NOA to HDEHP gave homogeneous and transparent liquid samples of increasing viscosity in the $0 \leqslant X_{NOA} \leqslant 0.43$ range whereas the sample at $X_{NOA} = 0.5$ appears as a waxy solid. A further increase in X_{NOA} leads to biphasic samples up to $X_{NOA} = 0.92$. Being interested in the behaviour of monophasic surfactant mixtures we focused our investigation on samples in the $0 \leqslant X_{NOA} \leqslant 0.5$ range. It is of interest to note that, by mixing NOA and HDEHP, a moderate heating of the mixture is observed. This can be taken as a first clue of the occurrence of an exothermic acid–base reaction between HDEHP and NOA.

FT-IR spectra were acquired at 25 °C with a Spectrum One spectrometer (Perkin Elmer), using a cell equipped with CaF_2 windows. Each spectrum was the average of eight scans in the 900–4000 cm^{-1} wavenumber range at a spectral resolution of 0.5 cm^{-1}. By IR spectroscopy no detectable signal due to water OH stretching was found in all the studied samples. This confirmed the absence of residual water.

X-ray diffraction (XRD) data of samples were recorded at 25 °C by a Philips diffractometer (PW1050/39 X Change) equipped with a copper anode (Cu-Kα, 1.5418 Å). Liquid mixtures were loaded into a 1.5 mm internal diameter/0.01 mm wall width glass capillary (M. Muller, Rohrchen, Malsfeld) while the sample at $X_{NOA} = 0.5$ into a sample holder for solids. Then, samples were placed within the measurement compartment maximizing the signal to noise ratio.

SAXS measurements were carried out with the 5.2 L SAXS beamline at Elettra Synchrotron Light Laboratory, (Trieste, Italy).[6] The chosen angular range provided data for $q = 0.08$ to 7.5 nm^{-1} (q is the scattering vector equal to $4\pi \sin 2\theta/\lambda$, where θ is the scattering angle and λ is the X-ray wavelength 0.154 nm). The scattering intensities $I(q)$ from the samples, detected by an image plate detector, were corrected by subtracting the cell contribution.

The dielectric measurements were performed in the 10^{-3}–10^{6} Hz frequency range using a home made setup. The parallel plate capacitor used to characterize the sample's dielectric properties consisted of gold plated copper electrodes (diameter 13 mm) separated by a PTFE spacer (thickness ~1 mm). In order to measure the complex impedance of the system, the same measurement cell was connected to different instruments working on complementary and partially overlapping frequency ranges: a Solartron 1260 impedance/gain analyzer equipped with a SI1296 Dielectric Interface (1 mHz to 100 kHz), a precision capacitance bridge AH2700 A Andeen-Hagerling (50 Hz–20 kHz), and a precision LCR meter HP4284 A (20 Hz to 1 MHz). From the measured quantities both the real and the imaginary part of the complex permittivity (ε^*) of the sample were obtained as a function of frequency. The measurement cell was kept in a nitrogen atmosphere. A MICROMEGA temperature controller unit (Omega Engineering, Inc.) was used for the temperature control. Each measurement was carried out after a period of thermal stabilization of at least 30 min. The sample temperature was stable within ±0.02 °C during a complete frequency sweep. The typical reproducibility of the permittivity measurements, after repeated filling and mounting of the cell, was better than 2%. Since water absorption could affect properties such as conductivity this guarantees that the samples do not significantly absorb water from the atmosphere during the measurements. The complex permittivity is described as

$$\varepsilon^* = \varepsilon'(\omega) - i\left[\varepsilon''(\omega) + \frac{\sigma_{DC}}{\omega\varepsilon_0}\right] \quad (1)$$

where ε_0 is the permittivity of free space (8.854 10^{-14} F cm^{-1}) and ω is the angular frequency. The relative static permittivity (ε_R) was obtained from the frequency independent portion of $\varepsilon'(\omega)$ at low frequencies, while the static (direct-current) conductivity (σ_{DC}) was obtained from the observed ω^{-1} dependence of the permittivity imaginary part at low frequencies.

The samples for polarized optical microscopy were prepared by placing a drop of the liquid mixtures or a small piece of the waxy solid (for the sample at $X_{NOA} = 0.5$) between two

glass slides. The optical micrographs were taken with an Optika polarizing microscope at room temperature.

Results and discussion

IR data

A typical IR spectrum of NOA–HDEHP mixtures (X_{NOA} = 0.33) in the 1000–3600 cm^{-1} wavenumber range is shown in Fig. 2 where the spectra of pure NOA and HDEHP are also shown for comparison.

In the high wavenumber region of the pure NOA spectrum, the bands due to the NH_2 antisymmetric (about 3370 cm^{-1}) and symmetric (3290 cm^{-1}) stretchings can be seen. The broadness of these bands and the marked red shift with respect to those of free amines (3496 cm^{-1} and 3401 cm^{-1}, respectively)[7] suggest that NOA in the pure state is engaged in hydrogen bonded structures characterized by head–head interactions. Similar conclusions can be drawn by considering the position and broadness of the NH_2 bending mode occurring at about 1610 cm^{-1} as well as its overtone at about 3190 cm^{-1}, appearing as a shoulder of the symmetric stretching.[7]

On the other hand, in the spectrum of pure HDEHP, there are the three characteristic broad bands of medium intensity occurring at about 1691 cm^{-1}, 2320 cm^{-1} (with a shoulder at 2189 cm^{-1}) and 2650 cm^{-1}, due to the strongly hydrogen bonded POH group, and the HDEHP combination bands at 1230 cm^{-1} ($\nu_{as}(PO_4)$ + δ(POH)) and at 1033 cm^{-1} ($\nu_s(PO_4)$ + δ(POC)).[8–10]

Considering the spectra of all the mixtures, it must be noted that they cannot be rationalized in terms of the additive contributes of the two components, meaning that some interaction occurs. In particular, as emphasized in Fig. 2, the following can be easily noted:

(i) The disappearance of the NH_2 symmetric and antisymmetric stretching bands and the appearance of a very broad band, extending from 2500 cm^{-1} to 3200 cm^{-1} and overlapping the CH_2 and CH_3 symmetric and antisymmetric stretching bands. Such a band is attributable to the stretching vibrations of the protonated and strongly hydrogen bonded NH_3^+ group.[11–13]

(ii) The disappearance of the NH_2 scissor bending band at 1610 cm^{-1} and the appearance of two new bands at about 1545 cm^{-1} and 1640 cm^{-1}, due to the bending vibrations of the NH_3^+ group, whose intensities increase with X_{NOA} in the range $0 < X_{NOA} < 0.5$ (see Fig. 3).[11,13]

(iii) The disappearance of the bands at 1691 cm^{-1}, 2320 cm^{-1} and 2650 cm^{-1}, due to the strongly hydrogen bonded POH group, and some changes of position, shape and width of the combination bands ($\nu_{as}(PO_4)$ + δ(POH)) and ($\nu_s(PO_4)$ + δ(POC)) with X_{NOA} (see Fig. 4).

Taken all together, these features strongly indicate the occurrence of a significant transfer of the acidic proton of the HDEHP POH group to the basic NOA NH_2 group, implying a head–head bonding between these surfactants in the mixtures.

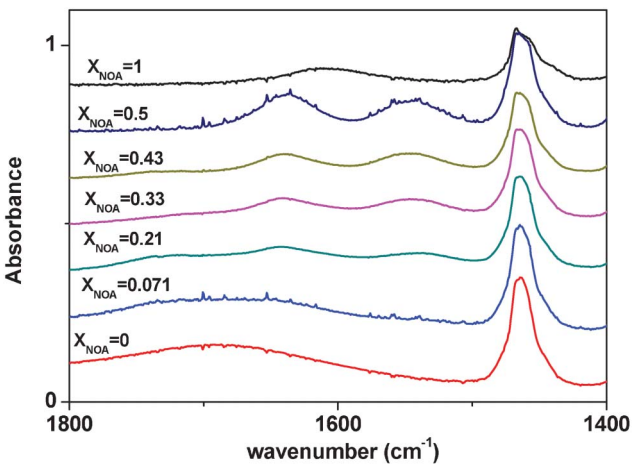

Fig. 3 X_{NOA} dependence in the 1400–1800 cm^{-1} spectral range of the intensities of the investigated samples.

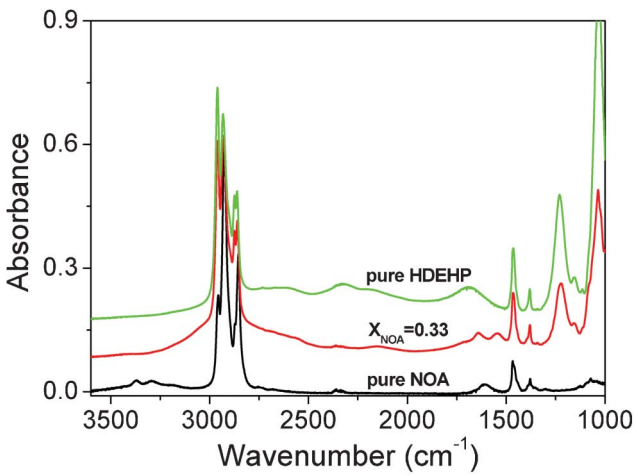

Fig. 2 IR spectra of pure NOA, pure HDEHP and the NOA–HDEHP mixture at X_{NOA} = 0.33 (spectra have been shifted to avoid crowding).

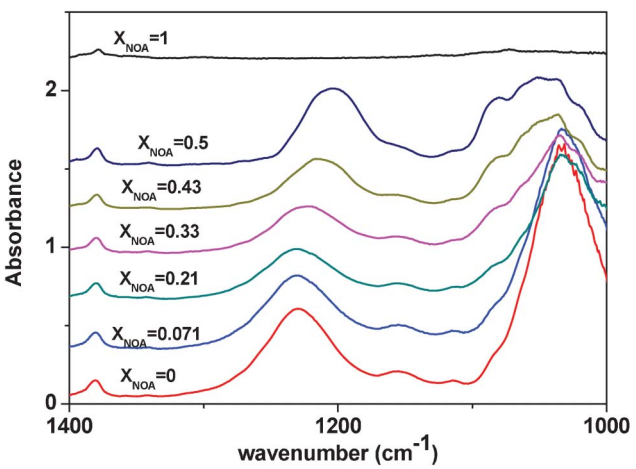

Fig. 4 X_{NOA} dependence in the 1000–1400 cm^{-1} spectral range of the intensities of the investigated samples.

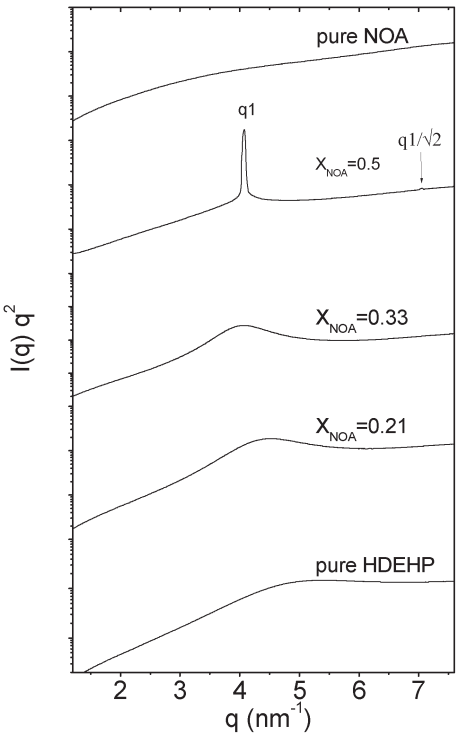

Fig. 5 SAXS profiles at 25 °C of some representative samples (Lorentz-corrected intensity, $I(q)q^2$, in log scale).

SAXS data

The structural evolution of the NOA–HDEHP mixtures, with composition $0 \leqslant X_{NOA} \leqslant 0.5$ and temperature 15 °C $\leqslant T \leqslant$ 70 °C, has been investigated by Small-Angle X-ray Scattering (SAXS). The Lorentz-corrected SAXS profiles ($I(q)q^2$) of some representative samples at 25 °C are shown in Fig. 5.

In the explored q window, a very diffuse maximum can be observed centred at q = 3.62–4.91 nm^{-1}, characteristic of the disordered liquid-like conformation of paraffin-based mesostructures containing mainly alkyl chains, clearly indicating the absence of a long range positional order. The most striking feature is the progressive change in position ($q1$) and Full Width at Half Maximum (FWHM1) with the composition and a disorder–order transition in the mesomorphous domain size at X_{NOA} = 0.5. In this sample, which appears as a waxy solid, an additional less intense feature occurring at 7.0 nm^{-1} is observed and will be discussed later.

The peak parameters ($q1$, FWHM1) of all the investigated samples at various compositions and temperature values are collected in Table 1 together with the corresponding characteristic distance ($d1$, $d1 = 2\pi/q1$)

As highlighted in Fig. 6a, the characteristic distance $d1$ is almost insensitive to the temperature, it increases with X_{NOA} up to X_{NOA} = 0.33 and then smoothly decreases up to X_{NOA} = 0.5. Taking into account that the scattering peak can be ascribed to the existence of local structures formed by surfactant head groups where the molecules are oriented in tail–head/head–tail configurations, the observed $d1$ values can be identified with the distance between these domains. Then, the observed behaviour is the result of two counteracting effects: (i) the progressive substitution of HDEHP with NOA (which has a longer alkyl chain than HDEHP) tends to enlarge the distance $d1$, an effect predominant at low X_{NOA} values; and (ii) the strong HDEHP–NOA head-to-head acid–base interactions tend to strengthen the local structures, leading to a decrease of $d1$, which instead is predominant at $X_{NOA} \geqslant 0.33$.

As regards FWHM1, which can be interpreted as an indicator of the degree of structural disorder, it can be noted that this parameter is quite insensitive to temperature and shows a sudden jump at X_{NOA} = 0.5, pointing out a disorder–order transition (see Fig. 6b). It can be postulated that the progressive increase in HDEHP–NOA nanodomain number density with X_{NOA} has caused at this composition a macroscopic scale transition due to a cooperative rearrangement which ultimately triggers a disorder–order transition.

It is important to note that self-assembly is an entropically hindered process, so the local structure formations can only be driven by a favourable enthalpic term. In this respect, the scarce temperature impact on $d1$ and FWHM1 values in the investigated temperature range suggests that the intermolecular stabilising interactions sustaining the local structures are much larger than the kT term and can be traced back to strong head–head interactions and relatively weak tail–tail ones. These structures can be viewed as formed by a floppy domain composed by the surfactant alkyl chains surrounding a stiff domain, whose stiffness increases with X_{NOA}, constituted by the surfactant head groups.

As for the feature occurring at about 7.0 nm^{-1} in the SAXS pattern of the sample at X_{NOA} = 0.5, it will be considered in the following section.

Table 1 $q1$, FWHM1 and $d1$ values for the investigated samples as a function of sample composition and temperature

X_{NOA}	10 °C			25 °C			40 °C			55 °C			70 °C		
	$q1$ (nm^{-1})	FWHM1 (nm^{-1})	$d1$ (nm)	$q1$ (nm^{-1})	FWHM1 (nm^{-1})	$d1$ (nm)	$q1$ (nm^{-1})	FWHM1 (nm^{-1})	$d1$ (nm)	$q1$ (nm^{-1})	FWHM1 (nm^{-1})	$d1$ (nm)	$q1$ (nm^{-1})	FWHM1 (nm^{-1})	$d1$ (nm)
0	4.91	2.59	1.28	4.91	2.64	1.28	4.90	2.64	1.28	4.92	2.64	1.28	4.91	2.69	1.28
0.071	4.67	2.21	1.34	4.67	2.23	1.34	4.67	2.27	1.34	4.67	2.28	1.34	4.67	2.28	1.34
0.21	4.37	1.44	1.44	4.37	1.43	1.44	4.38	1.49	1.43	4.38	1.50	1.43	4.38	1.52	1.43
0.33	4.00	0.90	1.57	4.01	0.92	1.57	4.02	0.94	1.56	4.03	0.96	1.56	4.03	0.97	1.56
0.43	4.00	0.90	1.57	4.01	0.92	1.57	4.02	0.94	1.56	4.03	0.97	1.56	4.03	0.98	1.56
0.50	4.08	0.05	1.54	4.08	0.05	1.54	4.06	0.05	1.55	4.05	0.05	1.55	4.05	0.04	1.55
1	3.65	1.55	1.72	3.62	2.1	1.74	3.55	2.2	1.77	3.57	1.73	1.76	3.54	1.8	1.77

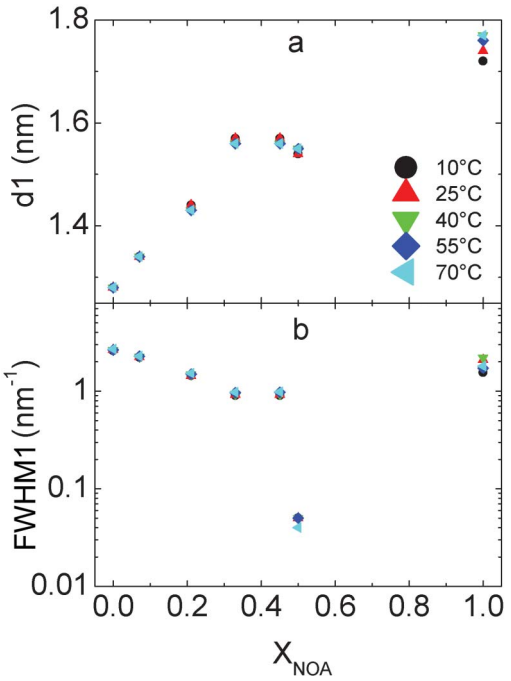

Fig. 6 X_{NOA} dependence at various temperatures of $d1$ (panel a) and FWHM1 (panel b, log scale).

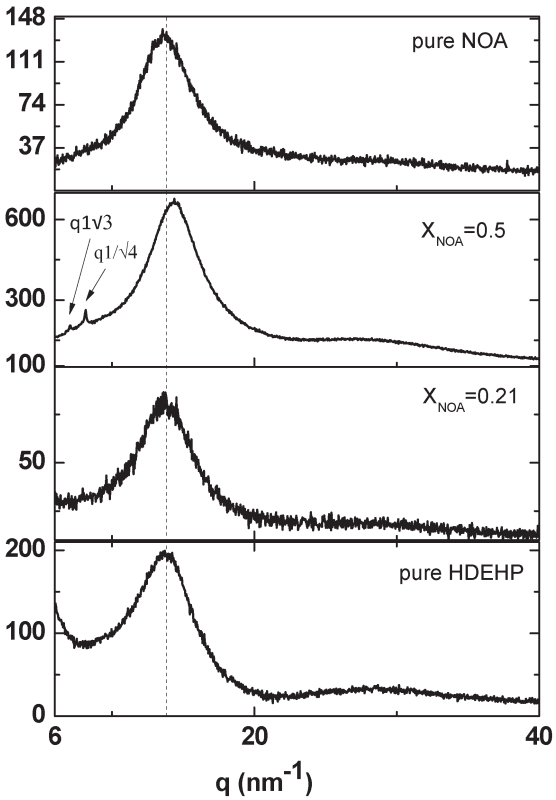

Fig. 7 WAXS profiles of some representative samples at 25 °C.

WAXS data

To gain further structural information, the WAXS spectra of all the samples at 25 °C have been collected. Some representative spectra in the 6 nm^{-1} ⩽ q ⩽ 40 nm^{-1} range are shown in Fig. 7.

It can be noted that the diffractograms are characterized by a broad peak located at about q = 13 nm^{-1}, which is characteristic of the disordered liquid-like conformation of paraffin-based mesostructures containing mainly alkyl chains and is ascribed to the typical intermolecular distance of separation perpendicular to the chains.[14,15] Its position ($q2$, see Table 2) is quite composition independent in the range 0 ⩽ X_{NOA} ⩽ 0.5 and corresponds to a distance of 0.44–0.46 nm. The fact that no marked change in the peak position and Full Width at Half Maximum (FWHM2) occurs, indicates that, including the X_{NOA} = 0.5 sample, the mean molecular conformation is preserved and the structural disorder is almost unaffected.

Moreover, only the diffractogram of the sample at X_{NOA} = 0.5 displays the presence of two features at q = 7.04 nm^{-1} and 8.14 nm^{-1}, corresponding to interplanar distances of 0.89 and 0.77 nm. Since these peaks occur at $q1\sqrt{3}$ and $q1\sqrt{4}$ where $q1$ corresponds to the interplanar distance of 1.54 nm^{-1} observed in the SAXS spectrum, it can be concluded that this sample forms a reverse hexagonal bidimensional structure, an arrangement frequently observed in pure dichained surfactants.[16–19]

Taking into account this geometry, the lattice parameter (a) through the relation $q(10) = 4\pi/3a$ turns out to be a = 1.78 nm, so that a schematic representation of the building block of the local structures of the X_{NOA} = 0.5 sample can be sketched (see Fig. 8). Since the mean domain size of the X_{NOA} = 0.5 sample, derived from the Full Width at Half Height by the Scherrer's equation is 126 nm, it must be noted that the typical local structure of this sample is constituted by a stacked arrangement of many of these building blocks.

Polarized optical microscopy data

Further support to the SAXS and WAXS results was achieved by polarized optical microscopy. In fact, all the liquid samples do not show any feature in the polarized optical microscope confirming the absence of long range structures. On the other hand, the sample at X_{NOA} = 0.5 is characterized by a rich colour texture at crossed polarizing glasses typical of hexagonal phases. Fig. 9 shows two typical micrographs.

Table 2 WAXS peaks and structural parameters of the investigated samples

X_{NOA}	$q2$ (nm^{-1})	Intermolecular distance (nm)	FWHM2 (nm^{-1})
0	13.9	0.45	4.7
0.071	13.7	0.46	3.7
0.21	13.9	0.45	3.7
0.33	13.5	0.46	3.3
0.43	13.7	0.46	3.1
0.50	14.3	0.44	3.4
1	13.8	0.46	3.7

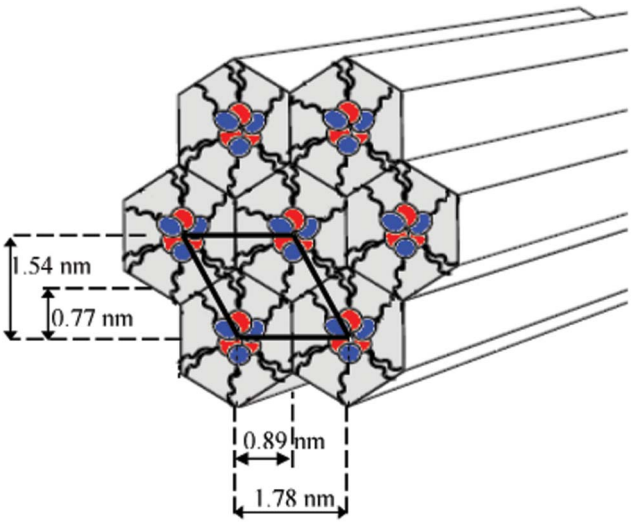

Fig. 8 Schematic representation of the X_{NOA} = 0.5 sample structure building block (the blue circle indicates the NOA head group and the red one the HDEHP head group). Thick lines delimit the unit cell.

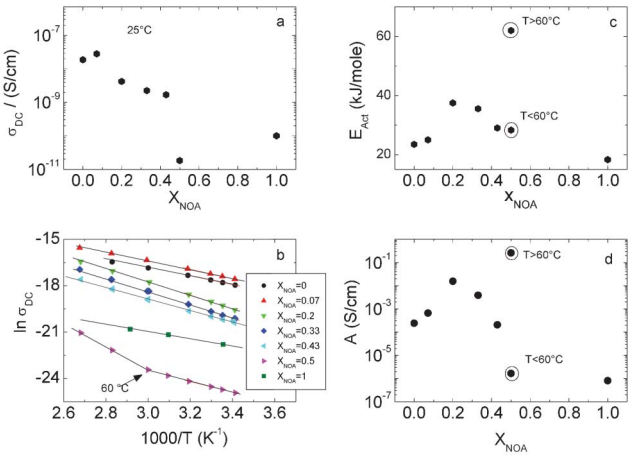

Fig. 10 Conductivity values (log scale) as a function of X_{NOA} (a); Arrhenius plots (b); activation energy (E_{act}) and pre-exponential factor (A) as derived by the Arrhenius plot, as a function of X_{NOA}, (c) and (d) respectively.

Conductivity and dielectric data

The conductometric behavior of HDEHP–NOA mixtures as a function of X_{NOA}, shown in Fig. 10a, is characterized by an initial conductivity increase followed by a decrease. This trend can be attributed to two contributions: an increase in charge carriers with X_{NOA} counteracted by a slowing down of molecular dynamics due to the intermolecular proton transfer.

Interestingly, the waxy sample at X_{NOA} = 0.5 markedly deviates from the observed trend showing a pretty suppressed conductivity consistent with the hypothesis that long range proton transfer in the HDEHP–NOA mixtures requires some re-orientation of the surfactant molecules which are evidently hindered in the waxy sample.

Conductivity data measurements carried out at various temperatures allow us to build the Arrhenius plots which are reported in Fig. 10b. The pretty linear trend in this plot for all the liquid samples indicates the goodness of the two-wells potential model, but the waxy sample at X_{NOA} = 0.5 behaves quite differently. This sample shows two linear trends with a break point at a temperature around 60 °C, indicating the occurrence of an abrupt change of the energetic barrier for the proton conduction. From these plots, the values of the apparent activation energy (E_{act}) and of the pre-exponential factor (A) can be extracted and are reported in Fig. 10 c and d, respectively. In these plots, the circled values at X_{NOA} = 0.5 indicate the two E_{act} and A values obtained from the Arrhenius plot in the two temperature ranges (below and above 60 °C). The values of E_{act} at $X_{NOA} < 0.5$ are in agreement with those for proton conduction.[4,20]

At $X_{NOA} < 0.5$ the trend of E_{act} is in full accordance with the structural features found by XRD: it reflects the effect of the progressive substitution of HDEHP with NOA (characterized by a longer alkyl chain) involving an increase in $d1$ and consequently in E_{act} due to an increased distance between the two wells of potential in the proton jump; this effect is joined with a strengthening of the NOA–HDEHP head-to-head interaction leading to a decrease of $d1$ and E_{act}. The first effect prevails at lower X_{NOA} values while the second becomes more effective at higher X_{NOA}.

Looking at the pre-exponential factor (A), it is worth noting that the physical meaning of A can be ultimately traced back to the charge carrier density: its increase with X_{NOA} in the low-X_{NOA} regime is obviously given by the progressive substitution

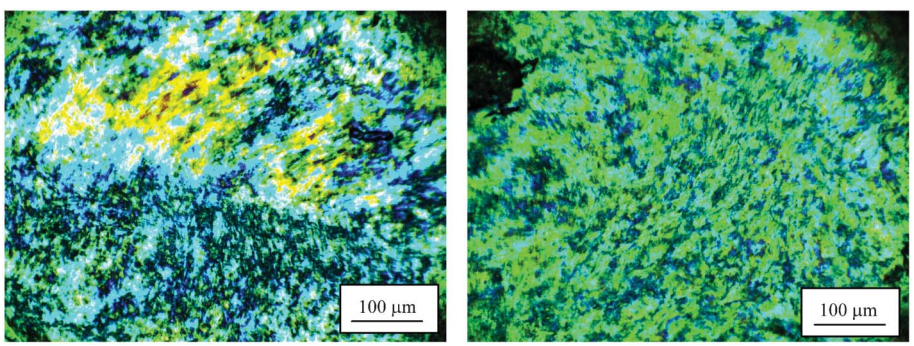

Fig. 9 Typical polarized optical micrographs of the sample at X_{NOA} = 0.5.

of HDEHP with NOA, with the HDEHP-to-NOA proton transfer increasing the number of "free" protons available for migration. After a further increase in X_{NOA} this effect is then suppressed by the strengthening of the NOA head–HDEHP head interaction hindering molecular re-orientation and consequently decreasing the number of "free" protons available for migration. It is interesting to note that the maxima of E_{act} and A occur at X_{NOA} = 0.2, which is slightly different from the maxima in $d1$ and FWHM1 as probed by SAXS, as a consequence of the fact that the two techniques probe different aspects of the same phenomenon.

Concerning the X_{NOA} = 0.5 sample, characterized by a mean domain size much larger than those of liquid samples, its peculiar behaviour can be rationalized by hypothesizing that proton migration occurs *via* proton jumps within a domain and from a domain to a neighbouring one; at high temperature the intra-domain conductivity dominates (characterized by high E_{act} and A values) whereas at low temperature the inter-domain conductivity dominates (characterized by low E_{act} and A values).

As to the static dielectric constant (ε_R), its composition dependence is reported in Fig. 11a. The behavior is similar to that of the conductivity, being the only value for X_{NOA} = 0.5 markedly different from all the others; in this sample, the particularly high value of ε_R indicates its enhanced orientational polarization due to the presence of extended $\cdots NH_3^+$–PO_4^-–NH_3^+–$PO_4^-\cdots$ networks. As a deeper insight, the X_{NOA} dependence of ε_R also reflects the structural and dynamical changes of the local surfactant head group domains, with a slight decrease in the low-X_{NOA} regime, a minimum at X_{NOA} = 0.2 and a successive increase with further increments of X_{NOA}.

Moreover, the temperature dependence of ε_R is shown in Fig. 11b as a function of the inverse temperature, a dependence generally explored in the literature due to the Kirkwood equation, whose slope can be taken as an indication of the orientational correlation between neighboring molecular dipoles.[21] All samples except for that at X_{NOA} = 0.5 show a linear trend (the slope b values are reported in Fig. 11c) in the whole temperature range. Taking into account that the main dipolar contribution of the surfactant molecules is due to their head groups, the observed b trend of the liquid samples probes the behavior of the orientational correlation between neighboring surfactant head groups.

On the other hand, the X_{NOA} = 0.5 sample shows two linear trends with a break point at a temperature around 60 °C (in Fig. 11c the circled b values at X_{NOA} = 0.5 indicate the two values obtained in the two temperature ranges: below and above 60 °C), indicating that at a temperature lower than 60 °C an enhanced dipole–dipole correlation due to the Onsager field occurs.[22]

This may be considered a further confirmation of the structuring occurring at X_{NOA} = 0.5. In particular the increased dipole correlation is consistent with the hypothesis that long-range structures, involving extended $\cdots NH_3^+$–PO_4^-–NH_3^+–$PO_4^-\cdots$ networks, are formed. It may be argued that, below a critical temperature, a change from uncorrelated single molecular dipole dynamics to strongly correlated NH_3^+–PO_4^- ones takes place.

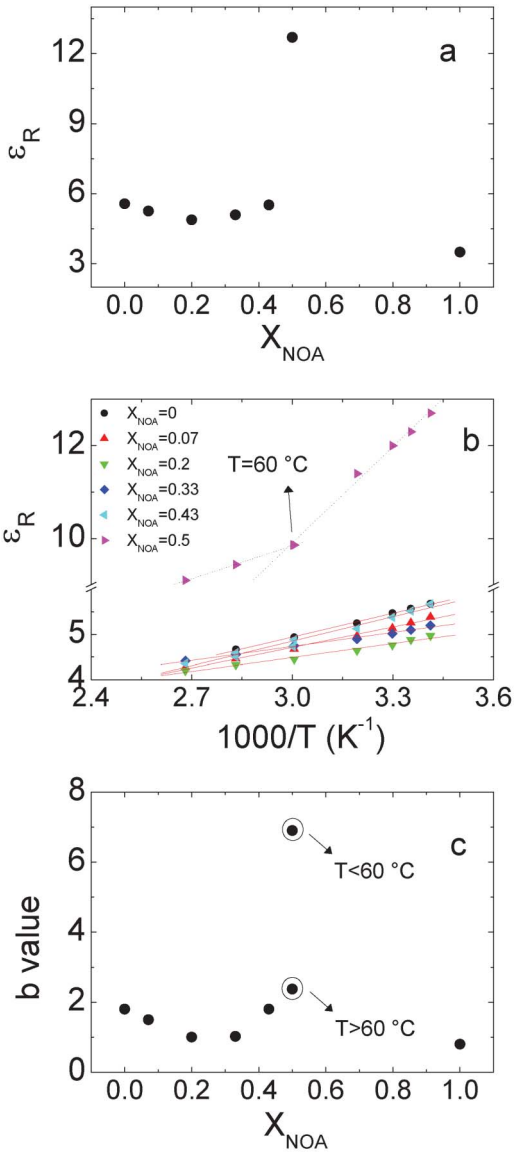

Fig. 11 Dielectric constant (ε_R) as a function of X_{NOA} at 25 °C (a); ε_R as a function of the inverse temperature (b); b value (see text) as a function of X_{NOA} (c).

As a conclusion, dielectric measurements reveal that the dynamical features consistently reflect the structural ones derived by IR and X-ray investigations, and that the progressive addition of NOA to HDEHP causes dramatic structural and dynamic effects when the critical composition X_{NOA} = 0.5 is reached. Given the acidic and basic character of HDEHP and NOA, respectively, intermolecular H-bonds are established, with a definite proton transfer from the acidic HDEHP to the basic NOA. This interaction, which usually triggers the formation of composition-dependent local structures in surfactant-based liquid mixtures,[3–5] does not seem to cause here the emergence of an enhanced conductivity. This difference with other systems may be understood by comparison with homologous molecules.

In a previous paper[3] we highlighted the formation of extended structures when HDEHP was mixed with bis(ethylex-

yl)amine (BEEA), an amphiphilic molecule which differs from the NOA used in this paper only by the alkyl chains: two and branched in BEEA, single and linear in NOA.

In our case, NOA, having the same amine group as the polar head but only a single and linear alkyl chain as the apolar part, can better fit the local HDEHP structure thanks to a more favorable steric hindrance, so that tighter and longer structures can be formed. Thus, the structural change with the formation of an extended hexagonal phase when the NOA-to-HDEHP ratio reaches the stoichiometry of 1 : 1 is abrupt and gives a material, differently from HDEHP–BEEA mixtures, with arrested dynamics and a suppressed conductivity as a consequence of the delicate balance between mutual interactions and steric effects.

Conclusions

Information on the structural and dynamic features of bis(2-ethylhexyl) phosphoric acid (HDEHP)–*n*-octylamine (NOA) mixtures have been gained by SAXS, WAXS, IR, dielectric spectroscopy and polarized optical microscopy. Data analysis shows a continuous variation of the physico-chemical properties of the mixtures with their composition interrupted by an abrupt variation at X_{NOA} = 0.5, which macroscopically corresponds to a transition from a transparent liquid to a waxy solid. Interpretation of all the experimental data at a molecular level allowed to rationalize such a composition-induced phase transition in terms of the synergetic effect of the progressive increase in size, number density and lifetime of ordered nanodomains with X_{NOA}. The driving force of this percolative behaviour has been identified in the HDEHP to NOA proton transfer due to the different acid–base character of these surfactants together with the reduced steric hindrance of the single linear alkyl chain of NOA which can better fit the structure of HDEHP. Thus, the observed enhancement of the structural order with X_{NOA} has been explained as due to the progressive substitution in the local structure of loosely bonded HDEHP–HDEHP aggregates with strongly hydrogen bonded NOA–HDEHP ones. Moreover, the absence of a significant temperature effect on these local structures suggests that their potential energy is much larger than the *kT* term.

From a general prospective, this investigation emphasizes the role of chemical structures in regulating the intermolecular interactions between surfactants in liquid mixtures which strongly affect their assembly and ultimately their macroscopic properties.

Acknowledgements

Financial support from MIUR 60% is gratefully acknowledged. The authors would like to acknowledge Dr H. Amenitsch (Elettra Synchrotron Light Laboratory, Italy) for assistance during the Small Angle X-ray Scattering experiments.

References

1 M. Yamada and I. Honma, *J. Phys. Chem. B*, 2004, **108**(18), 5522.
2 K. Je-Deok and I. Honma, *Solid State Ionics*, 2005, **176**, 979–984.
3 P. Calandra, A. Ruggirello, A. Mele and V. Turco Liveri, *J. Colloid Interface Sci.*, 2010, **348**, 183–188.
4 P. Calandra, V. Turco Liveri, P. Riello, I. Freris and A. Mandanici, *J. Colloid Interface Sci.*, 2012, **367**, 280–285.
5 P. Calandra, A. Mandanici, V. Turco Liveri, M. Pochylski and F. Aliotta, *J. Chem. Phys.*, 2012, **136**, 064515.
6 H. Amenitsch, S. Bernstorff, M. Kriechbaum, D. Lombardo, H. Mio, M. Rappolt and P. Laggner, *J. Appl. Crystallogr.*, 1997, **30**, 872–876.
7 J. K. Cooper, A. M. Franco, S. Gul, C. Corrado and J. Z. Zhang, *Langmuir*, 2011, **27**, 8486–8493.
8 M. I. Melnik, V. I. Spiryakov, V. T. Filimonov and E. A. Karelin, *J. Alloys Compd.*, 1998, **275**, 863–867.
9 L. D. Kurbatova and D. I. Kurbatov, *Russ. J. Appl. Chem.*, 2007, **80**, 2028–2030.
10 A. Ruggirello and V. Turco Liveri, *J. Colloid Interface Sci.*, 2003, **258**, 123–129.
11 D. Cook, *Can. J. Chem.*, 1964, **42**(10), 2292–2299.
12 R. A. Heacock and L. Marion, *Can. J. Chem.*, 1956, **34**(12), 1782–1795.
13 X. Jiang, Y. Yang, S. Sun, Z. Yin, X. Wang and M. Bao, *J. Phys. Chem. B*, 1999, **103**, 8657–866.
14 G. A. N. Gowda, H. Chen, C. L. Khetrapal and R. G. Weiss, *Chem. Mater.*, 2004, **16**, 2101–2106.
15 G. B. Stewart and R. M. Morrow, *Phys. Rev.*, 1927, **30**, 232–244.
16 P. Ekwall, L. Mandell and K. Fontell, *J. Colloid Interface Sci.*, 1970, **33**, 215.
17 A. Longo, A. Ruggirello and V. Turco Liveri, *Chem. Mater.*, 2007, **19**, 1127–1133.
18 P. Calandra, G. Di Marco, A. Ruggirello and V. Turco Liveri, *J. Colloid Interface Sci.*, 2009, **336**, 176–182.
19 P. Calandra, A. Longo, V. Marcianò and V. Turco Liveri, *J. Phys. Chem. B*, 2003, **107**, 6724–6729.
20 T. Kasuga, M. Nakano and M. Nogami, *Adv. Mater.*, 2002, **14**, 1490–1492.
21 F. J. Arcega and J. M. Forniés-Marquina, *J. Phys. D: Appl. Phys.*, 1982, **15**, 1783–1793.
22 J. N. Murrell and A. D. Jenkins, Properties of liquids and solutions, John Wiley & Sons Ltd, Baffins Lane, Chichester, West Sussex, England, 2nd edn, 1994.